

# The synthesis of mesoporous $\text{Ce}_{1-x}\text{Zr}_x\text{O}_2$ by modified evaporation-induced self-assembly method

X. B. Zhao · F. Chen · J. You · X. Z. Li · X. W. Lu ·  
Z. G. Chen

Received: 2 October 2009 / Accepted: 8 March 2010 / Published online: 23 March 2010  
© Springer Science+Business Media, LLC 2010

**Abstract** Mesoporous  $\text{Ce}_{1-x}\text{Zr}_x\text{O}_2$  with high surface area was synthesized using a modified evaporation-induced self-assembly method that combined citric acid as complexing agent and cetyltrimethyl ammonium bromide as surfactant. The samples with different Ce/Zr molar ratio were characterized by thermogravimetry and differential thermal analysis, X-ray diffraction, transmission electron microscopy, selected area electron diffraction, Brunauer–Emmett–Teller (BET), and Barrett–Joyner–Halenda methods. It was found that when the Zr molar fraction was larger than 0.3, a mixture of cubic phase and tetragonal phase was formed.  $\text{Ce}_{0.7}\text{Zr}_{0.3}\text{O}_2$  solid solution had the largest BET surface area ( $217 \text{ m}^2 \text{ g}^{-1}$ ) and mesoporous structure. The catalytic performances of mesoporous  $\text{Ce}_{1-x}\text{Zr}_x\text{O}_2$  for CO oxidation were examined. Mesoporous  $\text{Ce}_{0.7}\text{Zr}_{0.3}\text{O}_2$  solid solution demonstrated the best catalytic activity due to the high surface area and an enhanced redox property caused by appropriate  $\text{Zr}^{4+}$  incorporation.

## Introduction

The first mesoporous silica MCM-41 was synthesized in 1992 by Mobil Oil using surfactants as templates [1, 2]. Subsequently, a variety of mesoporous inorganic oxides, such as  $\text{TiO}_2$ ,  $\text{ZrO}_2$ ,  $\text{CuO}$ ,  $\text{Nb}_2\text{O}_5$ , etc. [3–7], had been synthesized by various types of soft templates [8] (cationic, anionic, block copolymer) or hard templates [9] (mesoporous- $\text{SiO}_2$ , mesoporous-Carbon).  $\text{CeO}_2$  is an important rare earth oxide because of its use either as catalyst and/or oxygen storage/release component in the formulation of catalysts for the control of emissions from automobiles [10]. Several efforts have been made to fabricate pure mesoporous  $\text{CeO}_2$  or a new generation of mixed oxides based on  $\text{CeO}_2$  and  $\text{ZrO}_2$  [11–19]. Comparing with pure  $\text{CeO}_2$ ,  $\text{CeO}_2$ – $\text{ZrO}_2$  mixed oxides ( $\text{Ce}_{1-x}\text{Zr}_x\text{O}_2$  solid solutions) have improved features, such as thermal resistance [20], redox and oxygen storage property [21, 22], and catalytic activity at lower temperatures [23, 24]. To the best of our knowledge, Terribile et al. [25] have prepared mesoporous  $\text{CeO}_2$ – $\text{ZrO}_2$  oxide using cetyltrimethyl ammonium bromide (CTAB) as templating agent. Recently, mesoporous  $\text{Ce}_{1-x}\text{Zr}_x\text{O}_2$  solid solutions have been synthesized using tri-block copolymer surfactant Pluronic (P123) by fast solvent evaporation in petri dish and by direct calcinations [26]. Those materials, fabricated by the evaporation-induced self-assembly (EISA) process, have shown improved physicochemical properties and thermal stability, so that they could be employed directly for the respective purpose of the functional oxides, e.g., for catalyst or electrode. Here, we report the synthesis of mesoporous  $\text{Ce}_{1-x}\text{Zr}_x\text{O}_2$  with varying  $\text{Zr}^{4+}$  molar ratios via a modified EISA method in which citric acid is added as complexing agent. The redox catalysis activity of materials is investigated by the catalytic conversion of carbon monoxide to carbon dioxide.

X. B. Zhao (✉) · J. You · X. Z. Li · X. W. Lu  
Faculty of Materials Science and Engineering,  
Jiangsu Polytechnic University, Changzhou 213164,  
People's Republic of China  
e-mail: zhaoxiaobing00@163.com

F. Chen  
Department of Materials Science and Engineering, Jiangsu  
University, Zhenjiang 212013, People's Republic of China

Z. G. Chen  
Department of Chemistry and Bioengineering, Suzhou  
University of Science and Technology, Suzhou 215011,  
People's Republic of China

## Experiment

### Sample synthesis

All reagents were of analytical grade and used without further purification. Typically, two solutions were prepared: one solution was prepared by dissolving 0.005 mol CTAB ( $\text{CH}_3(\text{CH}_2)_{15}\text{N}(\text{CH}_3)_3\text{Br}$ , SCRC) in 15 mL ethanol with stirring and the other solution was prepared by dissolving a total of 0.01 mol cerium nitrate hexahydrate ( $\text{Ce}(\text{NO}_3)_3 \cdot 6\text{H}_2\text{O}$ , SCRC), zirconium nitrate hexahydrate ( $\text{Zr}(\text{NO}_3)_4 \cdot 5\text{H}_2\text{O}$ , SCRC), which was added in proportion with  $\text{Zr}^{4+}$  molar fraction ranging from 0 to 0.5, and 0.005 mol citric acid monohydrate ( $\text{C}_6\text{H}_8\text{O}_7 \cdot \text{H}_2\text{O}$ , SCRC) in 5 mL deionized water. The cerium and zirconium solution was added, drop-by-drop, into the surfactant solution with a proper agitation to disperse the droplets. Afterward, the mixture was continuously stirred for 2 h to ensure thorough mixing, and then transferred to petri dish (90 mm in diameter). The dish was placed in an oven at 313 K for 5 days to form a gel. Calcination was carried out by slowly increasing temperature from room temperature to 573 K ( $2\text{ K min}^{-1}$  ramping rate) and heating at 573 K for 5 h. Decomposed  $\text{CeO}_2$  (named as s- $\text{CeO}_2$ ) was obtained by directly calcining  $\text{Ce}(\text{NO}_3)_3 \cdot 6\text{H}_2\text{O}$  at 773 K for 4 h.

### Material characterization

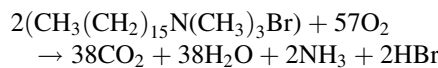
Thermal decomposition of the sample was studied by thermogravimetry and differential thermal analysis (TG-DTA) using a SDT Q600 TA instrument at a heating rate of  $10\text{ K min}^{-1}$  from room temperature to 800 K in air. The powder X-ray diffraction (XRD) patterns were recorded on Rigaku D/MAX-2500PC diffractometer with Cu target (40 kV, 40 mA) at a scanning rate of  $12^\circ \text{ min}^{-1}$ . For low angle ( $0.7\text{--}3^\circ$ ), X-ray diffraction was used with the same detector. The textural property and porosity of samples were studied by adsorption of nitrogen at 77 K with a Micromeritics ASAP-2010C instrument. Surface areas were calculated by the Brunauer–Emmett–Teller (BET) method, and pore size distribution was analyzed using the Barrett–Joyner–Halenda (BJH) method. The sample was determined by X-ray photoelectron spectroscopy (XPS) in an ion-pumped chamber (evacuated to  $1.3 \times 10^{-8}$  Torr) of an Axis Ultra (UK) spectrometer equipped with a focused monochromatized X-ray source ( $\text{Al-K}\alpha$ ,  $h\nu = 1486.6\text{ eV}$ ) at a power of 225 W. Transmission electron microscopy (TEM) and selected area electron diffraction (SAED) images were taken for morphology and particle size determination by using JEM-2010 transmission electron microscope, which operated at 200 kV.

### Catalytic test

Catalytic tests were carried out in a conventional fixed-bed quartz tube reactor (4.5 mm in inner diameter) between 473 and 823 K with feeding about 200 mg of the sample. The inlet gas composition was 1% CO and 5%  $\text{O}_2$  with  $\text{N}_2$  as balance, and the flow rate was kept at  $40\text{ mL min}^{-1}$ . The reactor effluent was analyzed using a Shanghai Haixin gas chromatograph (GC-950) with a TCD detector.

## Results and discussion

The inorganic/organic mixture was formed by the synthesis procedure described in section “[Sample synthesis](#).” The thermal analysis of the sample mixture is reported in Fig. 1. A weight loss of about 70% can be calculated from TG measurements in the temperature range of 300–800 K. In the same range, a series of thermal peaks are observed in the DTA trace. The TG curve shows that two small weight losses correspond to removal of residual solvent and decomposition of acetate groups and citric acid at about 320 and 450 K, respectively. A large obvious peak can also be found in the DTA profile with a large weight loss of about 40% in accordance with the quantity of surfactant in TG curve at about 550 K. It is suggested that the elimination of organic surfactants through combustion generates an exothermic reaction. The reaction of CTAB oxidation is as follows:



No peak is found on the DTA curve and no weight loss is observed on the TG curve after 550 K, indicating that the sample has been completely crystallized and all the organics have been removed.

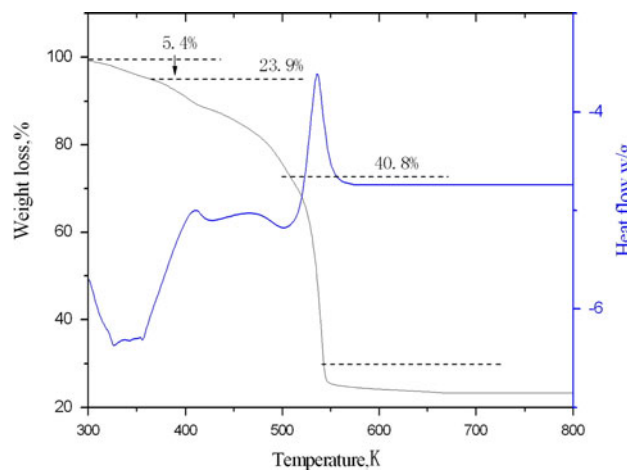


**Fig. 1** TG-DTA curves of the inorganic/organic mixture sample

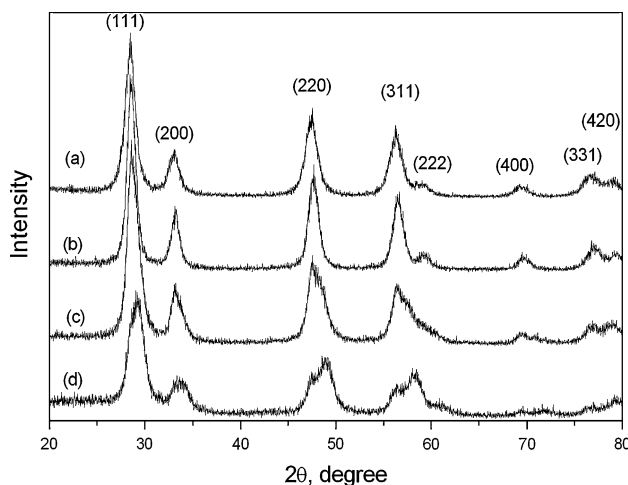


**Fig. 2** XRD patterns of  $\text{Ce}_{1-x}\text{Zr}_x\text{O}_2$ : (a)  $\text{CeO}_2$ , (b)  $\text{Ce}_{0.9}\text{Zr}_{0.1}\text{O}_2$ , (c)  $\text{Ce}_{0.7}\text{Zr}_{0.3}\text{O}_2$ , and (d)  $\text{Ce}_{0.5}\text{Zr}_{0.5}\text{O}_2$

Figure 2 shows the wide-angle PXRD patterns of the  $\text{Ce}_{1-x}\text{Zr}_x\text{O}_2$  ( $x = 0, 0.1, 0.3, 0.5$ ) composites after calcined at 573 K for 5 h.  $\text{Ce}_{1-x}\text{Zr}_x\text{O}_2$  solid solutions can exist in three stable phases (monoclinic (*m*), tetragonal (*t*), and cubic (*c*)) and two metastable phases (*t'*, *t''*) under different conditions [27]. In this study, PXRD patterns indicate that  $\text{Ce}_{1-x}\text{Zr}_x\text{O}_2$  has face-centered cubic structure (cerianite, JCPDS 34-0394) for compositions at  $x < 0.3$ , as shown in Fig. 2a and b, and no zirconia phases are detected by XRD. This may be due either to the formation of Ce–Zr oxide solid solutions or to the occurrence of amorphous zirconia. With increasing zirconium content, a progressive shift of the diffraction peaks to higher Bragg angles is observed. This shift indicates that part of zirconium species enters into the cerianite lattice and provokes the contraction of its unit cell, which is consistent with the formation of solid solutions [28, 29]. A systematic peak width broadening is also observed, indicating the occurrence of more defective cerianite lattice, lower degree of crystallinity, and smaller particle size. Around  $x = 0.3$ , the intensity of  $\text{CeO}_2$ -related peaks decreases, broad peaks attributed to cubic structure of zirconia appear as shown in Fig. 2c [30], but most of the powders retained the tetragonal phase and single solid solution structure. Furthermore, at  $x = 0.5$ , this phase obviously dominates in the two-phase mixture as shown in Fig. 2d, indicating the existence of separate  $\text{CeO}_2$  and  $\text{ZrO}_2$  phases.

The pore size distributions are reported in Fig. 3 for mesoporous  $\text{Ce}_{1-x}\text{Zr}_x\text{O}_2$  after calcination and concentrate below 10 nm. It can be observed that the pore size distribution for sample with  $x = 0.3$  has narrow pore distributions covering the range of 3–5 nm with a maximum at around 4.5 nm. A visible shift can be noted for other samples, since the maximum for pore distribution has become smaller. Some textural properties of the samples

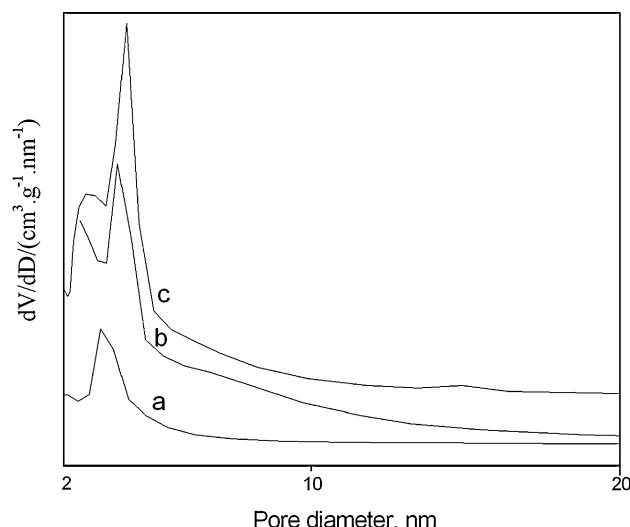


**Fig. 3** Pore size distribution of  $\text{Ce}_{1-x}\text{Zr}_x\text{O}_2$ : (a)  $\text{CeO}_2$ , (b)  $\text{Ce}_{0.9}\text{Zr}_{0.1}\text{O}_2$ , and (c)  $\text{Ce}_{0.7}\text{Zr}_{0.3}\text{O}_2$

**Table 1** Surface area and pore size of  $\text{Ce}_{1-x}\text{Zr}_x\text{O}_2$  samples

Samples	$\text{CeO}_2$	$\text{Ce}_{0.9}\text{Zr}_{0.1}\text{O}_2$	$\text{Ce}_{0.7}\text{Zr}_{0.3}\text{O}_2$	$\text{Ce}_{0.5}\text{Zr}_{0.5}\text{O}_2$
Surface area ( $\text{m}^2 \text{g}^{-1}$ )	205	211	217	135
Average pore size (nm)	3.5	4.0	4.2	1.3

are given in Table 1. The sample with  $x = 0.3$  has the largest BET surface area and the maximum average pore size, which is probably attributed to a positive physico-chemical contribution and good thermal resistance from adding Zr dopant to an optimal amount with no appreciable crystal structural and morphological changes. The surface area of the product by the modified EISA method is larger than the one prepared by the previous EISA method [26]. It is rationalized that in this modified EISA method the citric acid forms a complex compound in solution aligned with the  $\text{Ce}^{3+}$  and  $\text{Zr}^{4+}$  species, which aids to suppress the hydrolysis rate of inorganic ion and enhance the condensation and cross-linking of  $\text{Ce}(\text{Zr})-\text{O}-\text{Ce}(\text{Zr})$  bonds.

Figure 4a shows typical XPS survey spectrum of the mesoporous  $\text{Ce}_{0.7}\text{Zr}_{0.3}\text{O}_2$ . Core levels of Ce 4d, Zr 3d, Zr 3p, Zr 3s, C 1s, O 1s, and Ce 3d can be identified, and no peaks ascribable to N 1s are observed, suggesting that the  $\text{NO}_3^-$  and CTAB impurity are not present in the sample. The complex spectrum of Ce 3d can be decomposed into eight components with the assignment as defined in Fig. 4b. The bands labeled as  $v$  represent collectively Ce 3d<sub>5/2</sub>, and the bands labeled as  $u$  represent Ce 3d<sub>3/2</sub>. The bands labeled as  $u''$  and  $v''$  are attributed to  $\text{Ce}^{4+}$ . The  $u$ ,  $v$  and  $u''$ ,  $v''$  doublets are shakedown features resulting from transfer of one or two electrons from a filled O 2p orbital to

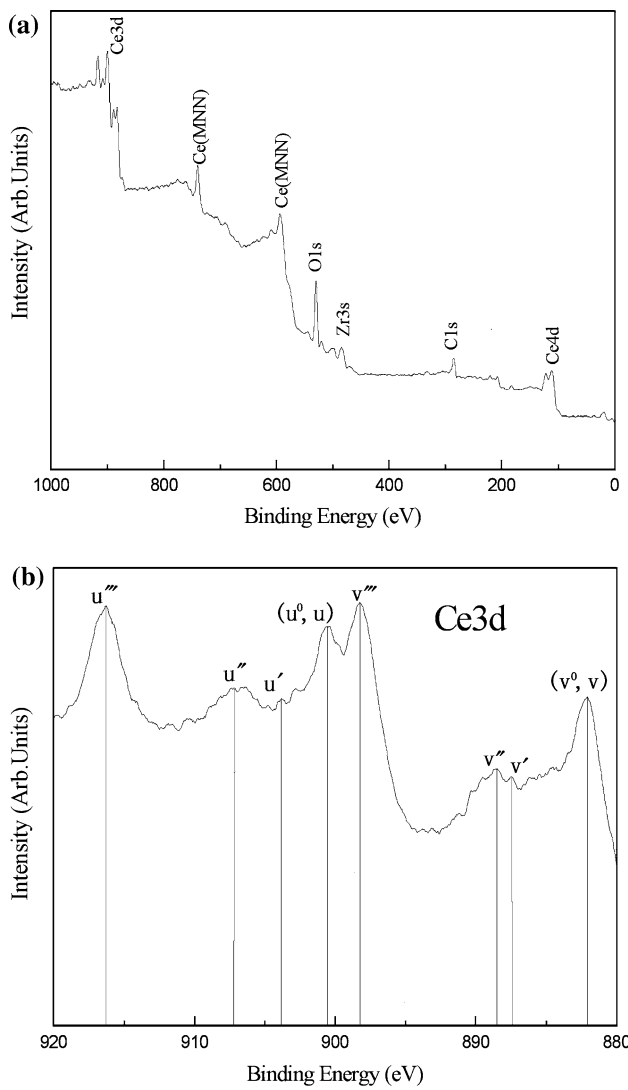


**Fig. 4** XPS spectra of mesoporous  $\text{Ce}_{0.7}\text{Zr}_{0.3}\text{O}_2$ : **a** Survey. **b** Ce 3d

an empty Ce 4f orbital. The bands labeled as  $v'$  and  $u'$  are due to the presence of  $\text{Ce}^{3+}$  [31]. The spectra confirm that the cerium mainly exists as the Ce(IV) and Ce(III) oxidation states (881.85 eV) [32].

The low-angle XRD pattern of the mesoporous  $\text{Ce}_{0.7}\text{Zr}_{0.3}\text{O}_2$  is shown in Fig. 5a. A weak and relatively broad reflection in the low-angle region is observed, and no other small-angle peaks are discernible, suggesting that the oxides synthesized from CTAB template are mesoporous. This indicates that there is disorder in the structure, or at least that the order is limited to a few regions [14, 33–35]. The size and morphology of the same sample is analyzed from the TEM image (Fig. 5b). And the figure reveals that the mesostructure of the products is not as well organized as in the case of mesoporous silicon dioxide [8] and consists of pores with diameter ranging from 3 to 5 nm. The electron diffraction patterns recorded in selected-area mode

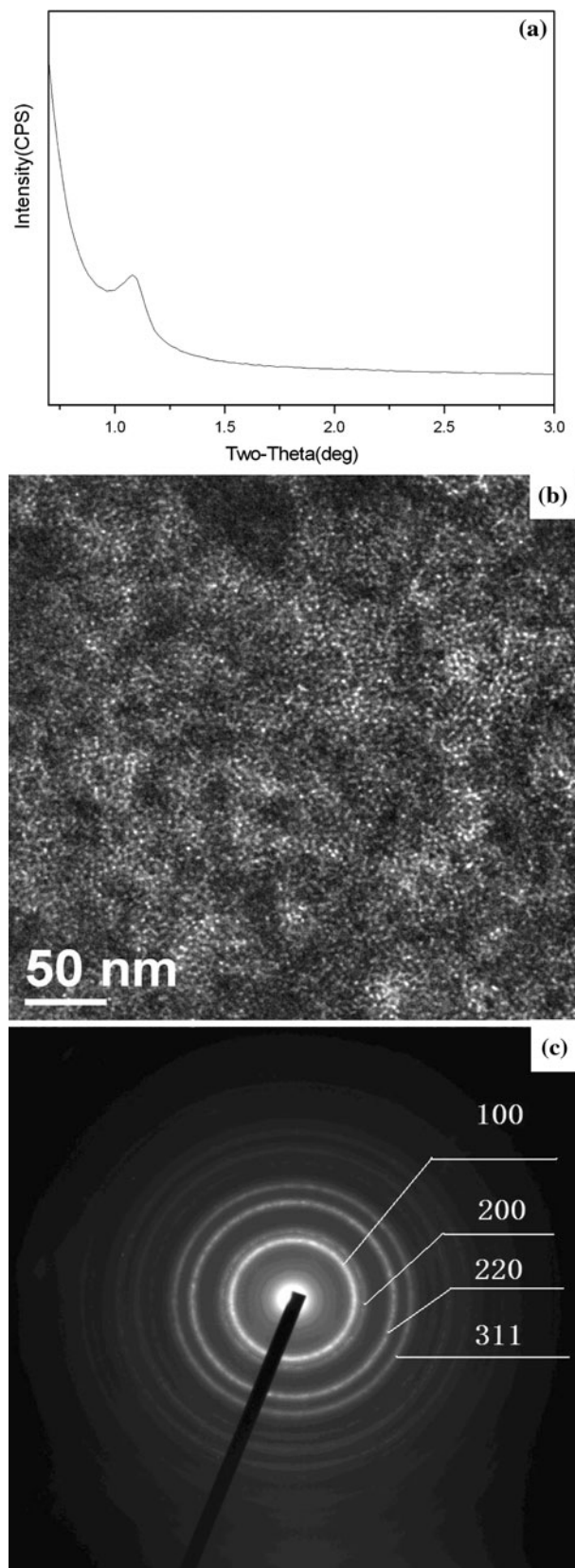


**Fig. 5** Low-angle XRD pattern **(a)**, TEM image **(b)**, and SAED spectrum **(c)** of mesoporous  $\text{Ce}_{0.7}\text{Zr}_{0.3}\text{O}_2$

(Fig. 5c) in several regions show smooth rings, which indicate that the sample is polycrystalline and is constituted by very small crystallites. It shows an aggregate and its corresponding SAED pattern along with an integrated intensity-spacing profile. The reciprocal spacings of the electron diffraction pattern and their relative intensity confirm cerium dioxide as the only fluorite cubic crystalline phase [18].

To test the catalytic activity of mesoporous  $\text{Ce}_{1-x}\text{Zr}_x\text{O}_2$  materials, the samples are used as catalysts and the reaction is as follows:



Figure 6 shows the catalytic activity profiles of CO conversion versus temperature. Prior to all catalytic experiments, samples were pre-treated in situ in reaction conditions identical to those of the second runs used for actual data collection. It is noted that the catalytic experiments are performed on samples of equal quantity (200 mg) to investigate differences of mesoporous materials with different Ce/Zr ratios, which may have an impact on the conversion rate. The surface area of decomposed s- $\text{CeO}_2$  prepared by  $\text{Ce}(\text{NO}_3)_3 \cdot 6\text{H}_2\text{O}$  calcined at 773 K is  $67 \text{ m}^2 \text{ g}^{-1}$ . Moreover, the surface area of mesoporous  $\text{Ce}_{1-x}\text{Zr}_x\text{O}_2$  is much larger than decomposed s- $\text{CeO}_2$ . There are reports that the addition of  $\text{ZrO}_2$  to  $\text{CeO}_2$  host can improve thermal stability and catalytic property [36–38]. From Fig. 6, it is found that the CO oxidation activity of mesoporous  $\text{Ce}_{1-x}\text{Zr}_x\text{O}_2$  is obviously higher than that of the ordinary s- $\text{CeO}_2$ . The mesoporous  $\text{Ce}_{0.7}\text{Zr}_{0.3}\text{O}_2$  shows notably lower conversion temperatures than other materials. It could be due to the fact that the introduction of  $\text{Zr}^{4+}$  may give rise to more oxygen vacancies without decreasing the active planes; also, the high surface area at

this optimal mole fraction is believed to contribute to the enhanced catalytic performance. However, the results in this study suggest that the doping effect is not linear. Excessive doping of  $\text{Zr}^{4+}$  into  $\text{CeO}_2$  results in the formation of mixed phases and the breakage of mesoporous structure, and the resulting catalyst has lower surface area and worse catalytic activity. It should be pointed out that a detailed study on the mechanism of the catalytic process of mesoporous  $\text{Ce}_{1-x}\text{Zr}_x\text{O}_2$  is under way.

## Conclusion

In summary, mesostructured  $\text{Ce}_{1-x}\text{Zr}_x\text{O}_2$  materials with high surface area were synthesized via a modified EISA method by choosing cerium nitrate and zirconium nitrate as inorganic species, CTAB as surfactant, and citric acid as complexing agent. The hydrolysis of inorganic ion in the solvent evaporation process was believed to be well controlled due to the existence of citric acid as complexing agent. The mesoporous solid solution was maintained when the  $\text{Zr}^{4+}$  molar fraction in  $\text{Ce}_{1-x}\text{Zr}_x\text{O}_2$  was not more than 0.3. However, more doping led to a mixture of cubic phases and tetragonal phases and decreased the surface area. The physicochemical contribution from  $\text{Zr}^{4+}$  doping and the structural evolution resulted in an optimal material at  $x = 0.3$  for CO conversion. More interestingly, the complexing action of the citric acid and  $\text{Ce}^{3+}$  ( $\text{Zr}^{4+}$ ) species was believed to not only suppress the hydrolysis rate of inorganic ion but also enhance the condensation and cross-linking of  $\text{Ce}(\text{Zr})-\text{O}-\text{Ce}(\text{Zr})$  bonds in this modified EISA method experiment. Moreover, this simple method, through the self-adjusted formation of mesostructure, could be applied to prepare a series of ceria-based mesoporous materials with various dopants.

**Acknowledgements** This work was financially supported by the National Science Foundation of China (NSFC20771047), Provincial Science Foundation of Jiangsu (BK2008541), and High-tech Project of Jiangsu (BE2008033).

## References

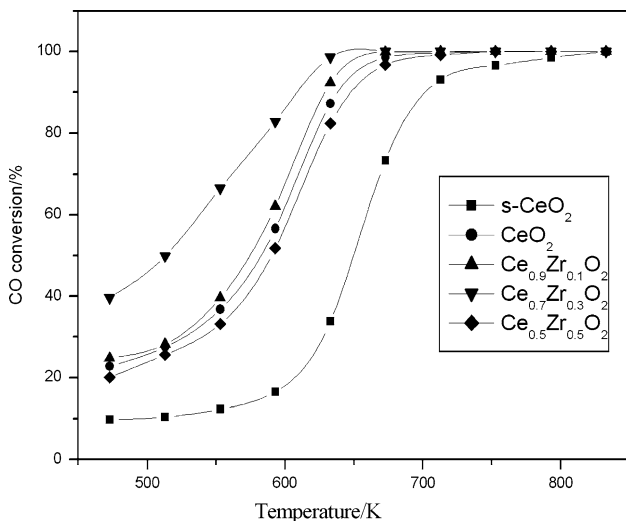


**Fig. 6** CO conversion profiles of  $\text{Ce}_{1-x}\text{Zr}_x\text{O}_2$  samples

- Beck JS, Vartuli JC, Roth WJ, Leonowicz ME, Kresge CT, Schmitt KD, Chu CT-W, Olson DH, Sheppard EW, McCullen SB, Higgins JB, Schlenker JLJ (1992) J Am Chem Soc 114:10834
- Kresge CT, Leonowicz ME, Roth WJ, Vartuli JC, Beck JS (1992) Nature 359:710
- Yang PD, Zhao DY, Margolese DI, Chmelka BF, Stucky GD (1999) Chem Mater 11:2813
- Yuan L, Gulians VV (2008) J Mater Sci 43:6278. doi: 10.1007/s10853-008-2904-7
- Wan Y, Yang HF, Zhao DY (2006) Acc Chem Res 39:423

6. Smarsly B, Gross D, Brezesinski T, Pinna N, Boissière C, Antonietti M, Sanchez C (2004) *Chem Mater* 16:2948
7. Lu DL, Katou T, Uchida M, Kondo JN, Domen K (2005) *Chem Mater* 17:632
8. Schüth F (2001) *Chem Mater* 13:3184
9. Tiemann M (2008) *Chem Mater* 20:961
10. Trovarelli A, Leitenburg CD, Dolcetti G (1997) *Chemtech* 6:32
11. Terrible D, Trovarelli A, Leitenburg C, Dolcetti G (1997) *Chem Mater* 9:2676
12. Lyons DM, Ryan KM, Morris MA (2002) *J Mater Chem* 12:1207
13. Lundberg M, Skarman B, Wallenberg LR (2004) *Micropor Mesopor Mater* 69:187
14. Laha SC, Ryoo R (2003) *Chem Commun* 2138
15. Corma A, Atinzar P, Garcia H, Chane-Ching JY (2004) *Nat Mater* 3:394
16. Shen WH, Dong XP, Zhu YF, Chen HR, Shi JL (2005) *Micropor Mesopor Mater* 85:157
17. Roggenbuck J, Schäfer H, Tsonecheva T, Minchev C, Hanss J, Tiemann M (2007) *Micropor Mesopor Mater* 101:335
18. Ni CY, Li XZ, Chen ZG, Li HY-H, Jia XQ, Shah I, Xiao JQ (2008) *Micropor Mesopor Mater* 115:247
19. Li XZ, Ni CY, Chen F, Lu XW, Chen ZG (2009) *J Solid State Chem* 182(8):2185
20. Pijolat M, Prin M, Soustelle M, Touret O, Nortier P (1995) *J Chem Soc Faraday Trans* 91:3941
21. Fornasiero P, Balducci G, Monte RD, Kasipar J, Sergo V, Gubitosa G, Ferrero A, Graziani M (1996) *J Catal* 164:173
22. Zamar F, Trovarelli A, Leitenburg CD, Dolcetti G (1996) *Stud Surf Sci Catal* 101:1283
23. Zamar F, Trovarelli A, Leitenburg CD, Dolcetti G (1995) *J Chem Soc Chem Commun* 965
24. Rao GR, Fornasiero P, Monte RD, Kasipar J, Vlaic G, Balducci G, Meriani S, Gubitosa G, Cremona A, Graziani M (1996) *J Catal* 162:1
25. Terrible D, Trovarelli A, Llorc J, Leitenburg CD, Dolcetti G (1998) *Catal Today* 43:79
26. Yuan Q, Liu Q, Song WG, Feng W, Pu WL, Sun LD, Zhang YW, Yan CH (2007) *J Am Chem Soc* 129(21):6698
27. Liang X, Wang X, Zhuang Y, Xu B, Kuang S, Li YD (2008) *J Am Chem Soc* 130:2736
28. Yashima M, Morimoto K, Ishizawa N, Yoshimura M (1993) *J Am Ceram Soc* 76:1745
29. Yashima M, Morimoto K, Ishizawa N, Yoshimura M (1993) *J Am Ceram Soc* 76:2865
30. Abdollahzadeh Ghom S, Zamani C, Nazarpour S, Andreu T, Morante JR (2009) *Sens Actuators B* 140:216
31. Wong GS, Vohs JM (2002) *Surf Sci* 498:266
32. Abi-aad E, Bechara R, Grimblot J, Aboukais A (1993) *Chem Mater* 5:793
33. Li J, Hao Y, Li H, Xia M, Sun X, Wang L (2009) *Micropor Mesopor Mater* 120:421
34. Velu S, Kapoor MP, Inagaki S, Suzuki K (2003) *Appl Catal A* 245:317
35. Kapoor MP, Raj A, Matsumura Y (2001) *Micropor Mesopor Mater* 44–45:565
36. Si R, Zhang YW, Xiao CX, Li SJ, Lin BX, Kou Y, Yan CH (2004) *Phys Chem Chem Phys* 6:1056
37. Teng ML, Luo LT, Yang XM (2009) *Micropor Mesopor Mater* 119:158
38. Singh P, Hegde MS (2008) *J Solid State Chem* 181:3248